Title

Conjunctival and Intrascleral Vasculatures Assessed Using Anterior Segment Optical Coherence Tomography Angiography in Normal Eyes

Authors

Akagi, Tadamichi
Uji, Akihito
Huang, Alex S
et al.

Publication Date

2018-12-01

DOI

10.1016/j.ajo.2018.08.009

Peer reviewed

HHS Public Access

Author manuscript

Am J Ophthalmol. Author manuscript; available in PMC 2019 December 01.

Published in final edited form as:

Am J Ophthalmol. 2018 December ; 196: 1–9. doi:10.1016/j.ajo.2018.08.009.

Conjunctival and Intrascleral Vasculatures Assessed Using Anterior-Segment Optical Coherence Tomography Angiography in Normal Eyes

Tadamichi Akagi[1], **Akihito Uji**[1], **Alex S. Huang**[2], **Robert N. Weinreb**[3], **Tatsuya Yamada**[1], **Manabu Miyata**[1], **Takanori Kameda**[1], **Hanako Ohashi Ikeda**[1], and **Akitaka Tsujikawa**[1]

[1]Department of Ophthalmology and Visual Sciences, Kyoto University Graduate School of Medicine, Kyoto, Japan

[2]Doheny and Stein Eye Institutes and Department of Ophthalmology, David Geffen School of Medicine, University of California Los Angeles, Los Angeles, CA

[3]Hamilton Glaucoma Center, Shiley Eye Institute, and Department of Ophthalmology, University of California San Diego, La Jolla, CA

Abstract

Purpose: To investigate conjunctival and intrascleral vasculatures using anterior-segment (AS) optical coherence tomography angiography (OCTA) in normal eyes.

Design: Cross-sectional study.

Methods: AS-OCTA images of the corneal limbus were acquired circumferentially using a swept-source OCT system in 10 eyes of 10 healthy subjects. AS-OCTA flow patterns with en face maximum projection were compared between the superficial (from the conjunctival epithelium to a depth of 200 μm) and deep (from a depth of 200 μm to 1000 μm) layers. The OCTA images were also compared with fluorescein scleral angiography and indocyanine green aqueous angiography images.

Quantitative parameters (vessel density, vessel length density, vessel diameter index, and fractal dimension) were compared among different locations.

Results: The OCTA vessel patterns differed between the superficial and deep layers. The superficial-layer flow signals showed centrifugal patterns from the limbus, whereas the deep-layer flow signals showed segmental patterns. The OCTA en face images with whole signals had a similar appearance to the scleral angiography images, whereas those in the deep layer showed a similar appearance to the aqueous angiography images. In the superficial layer, only the vessel

Corresponding author: Tadamichi Akagi, Department of Ophthalmology and Visual Sciences, Kyoto University Graduate, School of Medicine, 54 Shogoin Kawahara-cho, Sakyo-ku, Kyoto 606-8507, Japan, (Phone: +81-75-751-3248; Fax: +81-75-752-0933; akagi@kuhp.kyoto-u.ac.jp).

Supplemental Material available at AJO.com.

diameter index was significantly different among the locations ($P = 0.003$). In the deep layer, all four parameters differed significantly among the locations ($P < 0.001$ to $P = 0.003$).

Conclusions: OCTA is a promising tool for evaluating conjunctival and intrascleral vasculatures. It may also help in understanding ocular surface blood flow relevant to vascular and ocular surface diseases, as well as aqueous humor outflow.

Introduction

Several types of vessels are present in the peri-limbal conjunctiva and sclera.[1] Bulbar conjunctival vessels are primarily derived from the ophthalmic artery and could be affected by systemic diseases, such as diabetes[2] and systemic hypertension,[3] as well as other ocular conditions such as infection, allergy,[4] and dry eye.[5] The episcleral venous plexus and the deep and mid scleral venous plexuses lie under the conjunctiva. They are formed from anastomoses of the collector channels (arising from Schlemm's canal) with the ciliary venous plexus.[1, 6]

The conjunctival and episcleral vessels can be directly visualized using several types of imaging modalities, including fluorescent angiography.[7–14] However, non-invasive quantitative evaluation of these vessels at an intended depth has been difficult, and intrascleral vessels are often difficult to identify because of the opaque scleral tissue. Optical coherence tomography angiography (OCTA), a new technique for non-invasive imaging of the blood vessels,[15, 16] can obtain signals at arbitrary depths of tissues and offer the potential for such depth-resolved imaging. Previous studies have investigated the vessels of the posterior eye segments, such as the optic nerve head, retina, and choroid.[17–21] Although a few OCTA studies have investigated the vessels of the anterior segment (AS), such as the iris and cornea,[22–25] the potential of AS-OCTA has not been fully explored. AS-OCTA is supposed to be useful for various types of ocular or systemic diseases, including ocular-surface disorders and glaucoma, if it can assess the conjunctival and scleral vessels qualitatively and quantitatively.

In this study, we demonstrate the feasibility of imaging the conjunctival and intrascleral vasculatures using swept-source OCTA in normal participants and also compare the images to those obtained with fluorescein scleral angiography and indocyanine green (ICG) aqueous angiography.

Methods

This was a prospective cross-sectional study. This study was approved by the Institutional Review Board and Ethics Committee at Kyoto University Graduate School of Medicine, and was registered with the University Hospital Medical Information Network (UMIN) Clinical Trials Registry of Japan (UMIN000028853). All aspects of the study adhered to the tenets of the Declaration of Helsinki. After the study design, risks, and benefits of participation were thoroughly explained to the participants, written informed consent was obtained from them.

OCTA Participants

This study included 10 normal healthy volunteers with no history of ocular or systemic disease. The right eye of each participant was included.

AS-OCTA Examination

OCTA examination was performed using a swept-source OCT system (PLEX Elite 9000; Carl Zeiss Meditec, Dublin, CA, USA). This instrument has a central wavelength between 1040 and 1060 nm, a bandwidth of 100 nm, an A-scan depth of 3.0 mm in tissue, and a full-width at half-maximum axial resolution of approximately 5 μm in tissue. The instrument performs 100,000 A-scans/s. AS-OCTA images were acquired using the 10-diopter optical adaptor lens developed by Carl Zeiss Meditec. All OCTA scans were acquired by the same operator (TY).

OCTA Image Acquisition and Processing

For each participant, a 3 × 3-mm scan pattern was used to acquire AS-OCTA images of the corneal limbus in eight directions circumferentially, which consisted of 300 A-scans per B-scan repeated four times at each of the 300 B-scan positions. The size of this 3 × 3-mm scan pattern is correspond to typical “Retina” dimensions and approximately 6 × 6-mm in AS-OCTA images. The 6 × 6-mm scan image was also obtained by focusing on the corneal center as a guide for panoramic imaging. A panorama of AS-OCTA images was created from the eight scans (3 × 3 mm) for the whole circumference. It should be noted that the lateral resolution of the image was unknown because of the inaccuracy of the scan length, whereas the axial resolution could be defined as 5 μm/pixel.

En face images were generated using a built-in software (Ver. 1.6.0.21130; Carl Zeiss Meditec). Flattening was performed at the level of the conjunctival epithelium, which was misidentified as the inner limiting membrane by the software. The OCTA images from the conjunctival epithelium to a depth of 100 μm and from a depth of 100 μm to 200 μm from the conjunctival epithelium (Figure 1, Top far left and Top near left) showed similar features of the vasculature and characteristics different from the deeper OCTA images (from a depth of 200 μm to 300 μm and from a depth of 300 μm to 1000 μm from the conjunctival epithelium) (Figure 1, Top near right and Top far right). Superficial- and deep-layer flow images were developed with en face maximum projection from the conjunctival epithelium to a depth of 200 μm and from a depth of 200 μm to 1000 μm from the conjunctival epithelium, respectively (Figure 1, Bottom near right and Bottom far right). The projection-resolved algorithm in the built-in software was used when developing the deep-layer en face images. The superficial and deep layers mainly have conjunctival and intrascleral compositions, respectively. Schlemm’s canals of all participants were confirmed to be within the deep layer.

Quantitative Measurements

Vessel density, vessel length density, vessel diameter index, and fractal dimension of superficial- and deep-layer flows were measured in the 3 × 3-mm scan images in four

quadrants (nasal, temporal, inferior, and superior). For measurements, a 1024 × 1024-pixel rectangular box was cropped and binarized using a modified version of the previously reported method using ImageJ software (Wayne Rasband, National Institutes of Health, Bethesda, MD; available at http://rsb.info.nih.gov/ij/index.html) (Supplemental Figure 1).[26, 27] Briefly, after processing with a top-hat filter, images were skeletonized by processing the OCTA images through a band-pass filter. This was followed by binarization with intensity thresholding using Otsu's thresholding method for automatic binarization-level decisions.[28]

Vessel density was defined as the ratio of the area occupied by the vessels divided by the total area. Vessel length density, which represents the vessel length per unit area, was evaluated as described previously.[26, 27, 29] Vessel diameter index, which represents the average vessel caliber, was calculated by dividing the total vessel area in the binarized image (shown in Supplemental Figure 1, Middle) by the total vessel length in the skeletonized image (shown in Supplemental Figure 1, Right).[21, 27] Fractal dimension was calculated on the skeletonized image using ImageJ plugin software.[27, 30] The box-counting method was used for calculation. Fractal dimension could range from 0 to 2, and images with a more complex vessel branching pattern will have a higher fractal dimension. If the eyelid of the participant was included in the OCTA en face image, the area with the eyelid was carefully excluded from the analyses.

Scleral Angiography and Aqueous Angiography

To perform comparative assessments of OCTA images, fluorescein scleral angiography and ICG aqueous angiography was performed in different subjects.

Scleral angiography was performed on normal left eyes of two participants who were initially evaluated for neoplasms in their right eyes (57-year-old woman with a ciliary epithelial adenoma and 61-year-old man with a ciliary body melanoma).[14] These images were obtained using the Spectralis HRA+OCT (Heidelberg Engineering, Heidelberg, Germany) and a 55-degree lens. Three milliliters of 10% fluorescein (332.3 g/mol) (Akorn, Lake Forest, IL, USA) was delivered intravenously, and angiographic images were acquired focusing on the external sclera, as described previously.[14]

Aqueous angiography with ICG was performed on two individuals (a 72-year-old woman and a 54-year-old man) during scheduled cataract surgery using a customized arm (Spectralis HRA+OCT Flex module; Heidelberg Engineering) as described previously.[31, 32] Briefly, pharmaceutical-grade ICG (ICGREEN 25 mg, Akorn) was dissolved in 0.7 mL of the manufacturer-supplied solvent, followed by 5.6 mL of balanced salt solution to achieve a 0.4% concentration. After the introduction of ICG through an inferotemporal 1-mm side-port, fluorescent confocal scanning laser ophthalmoscopy-infrared images were acquired with the anterior segment module. A gravity-delivered constant pressure was set at approximately 18.7 mmHg.

Statistical Analysis

All values were presented as means ± standard deviation, where applicable. Differences in the four parameters (vessel density, vessel length density, vessel diameter index, and fractal dimension) among the four different locations (nasal, temporal, inferior, and superior) were evaluated using the analysis of variance (ANOVA). Post hoc analyses using Tukey's honestly significant differences were used to compare these four parameters between the locations. Differences in these four parameters between the superficial and deep layers were compared using the paired t-test. All analyses were performed using IBM SPSS Statistics 24 (IBM Corp., Armonk, NY, USA). *P* values less than 0.05 were considered statistically significant. In the post hoc analysis, the significance of differences between the locations was determined after Bonferroni correction.

Results

In each of the 10 eyes of 10 normal participants, the conjunctival and intrascleral vessels were well visualized using swept-source OCTA (Figure 2, Top left). These participants had an average age of 28.5 ± 7.1 years (range, 21–45 years). Seven participants were women.

The OCTA images with whole signals (Figure 2, Top left, Figure 3, Top row far left and Second row far left) showed very dense vasculature and quite similar appearance to the scleral fluorescein angiography images (Figure 3, Bottom far left and near left). Leakage of fluorescein was slightly observed from the vessels in the scleral angiography images, but not in the OCTA angiography images. In the superficial-layer en face OCTA images, the vessels circumferentially extended radially and smaller vessels existed among them homogeneously from the limbus to the periphery (Figure 2, Top right, Figure 3, Top row near left and Second row near left). The deep-layer flow images showed segmental patterns; that is, network-patterned dense intrascleral venous plexuses were present near the limbus and fewer vessels extended from the limbus to the periphery (Figure 2, Bottom left, Figure 3, Top row near right and Second row near right). The vessel patterns differed between the superficial and deep layers. The merged images with superficial- and deep-layer flows showed that the flow signals in those two layers could be well identified separately (Figure 2, Bottom right, Figure 3, Top row far right and Second row far right). The deep-layer flow images showed Y-shaped segmental flow patterns, which were quite similar to the aqueous humor outflow (AHO) images acquired using ICG (Figure 3, Bottom row near right and far right). All of 10 eyes analyzed in the current study showed the same characteristics in their OCTA images. Examples of OCTA panoramic images in subjects different from Figure 3 are shown in Supplemental Figure 2.

Vessel density, vessel length density, vessel diameter index, and fractal dimension in the superficial and deep layers are shown in Table 1. In the superficial layer, only vessel diameter index was significantly different among the locations ($P = 0.003$, ANOVA). The superficial vessel diameter index was the highest in the nasal quadrant. In the deep layer, all four parameters differed significantly among the locations ($P < 0.001$ to $P = 0.003$, ANOVA). Vessel density, vessel length density, or fractal dimension was higher in the nasal and temporal quadrants, whereas vessel diameter index was smaller in those quadrants.

Figure 4 shows the locations of the deep-layer OCTA flow signals. The OCTA flow signals corresponded to the low-intensity luminal episcleral or intrascleral structures in the OCTA B-scan image (Figure 4). The OCTA signals could not be detected in Schlemm's canal, and it was difficult to identify the collector channels (Figure 1, Bottom left, yellow arrowhead).

Discussion

The current study shows that swept-source OCTA can successfully visualize both the intrascleral and conjunctival vessels. The density, diameter, and pattern complexity of these vessels differed with depth and location. OCTA flow images with whole signals showed a similar appearance to the scleral angiography images, and deep-layer OCTA flow images had similar characteristics to aqueous angiography images.

Superficial-layer OCTA flow imaging mostly showed vessels extending centrifugally from the limbus and smaller vessels existing diffusely among them from the limbus to the periphery. The density and diameter of the superficial vessels were highest in the nasal quadrant (Table 1). Several external factors, such as ultraviolet radiation, wind, and dry atmosphere, might increase the density and diameter of the superficial vessels,[4, 5] whereas internal factors (systemic diseases such as diabetes and hypertension) also can affect the conjunctival vessels.[2, 3] In future studies, quantitative assessments of the conjunctival vessels using OCTA might be useful to investigate how these vessels are associated with various types of diseases.

Deep-layer flow imaging showed segmental flow patterns that were different from those of superficial-layer flow imaging. Quantitative assessments showed that the vessels in the nasal and temporal quadrants were denser, thinner, and more complex in pattern than those in the inferior or superior quadrant (Table 1). The venous plexuses in the deep and mid sclera and episclera are known to drain from Schlemm's canal through the collector channels.[1, 33] Therefore, the episcleral and intrascleral vessels have been of interest because of their potential for use in evaluating the function of the AHO pathway. Several studies have tried to visualize the posttrabecular AHO pathway in the eyes of living human subjects.[32, 34–39] However, in AS-OCT or computed tomography imaging, only luminal structures were identified as the AHO pathways, regardless of whether they were functional.[34–37, 40] Recently, Huang et al[31, 32] showed that aqueous angiography using ICG can visualize the AHO pathway. This method can be used to intraoperatively evaluate the functional AHO pathway of patients. Because the deep-layer flow images acquired using OCTA in the current study showed a similar appearance to the aqueous angiography images (Figure 3), there is a strong possibility that deep-layer OCTA signals include components of the functional post-trabecular AHO pathway. Although aqueous ICG angiography imaging reported by Huang et al has an advantage in its direct identification of the functional AHO pathway, its disadvantages are its relative invasiveness, the need to be performed in a non-physiological condition while in an operating room and the difficulty of quantitative evaluation. OCTA imaging has advantages in its non-invasiveness and convenience; it also is less-time-consuming and can be evaluated quantitatively. The OCTA flow images in this study were not directly compared with the aqueous angiography images in the same subjects. A direct comparison between these two methods would be helpful to better

understand the AHO pathway with AS-OCTA imaging in future studies. There also might be a possibility that AS-OCTA imaging can be used to assess the function of AHO pathway before trabecular glaucoma surgery in future.

In the current study, the OCTA signals could not be detected in Schlemm's canal and collector channels. OCTA signals are thought to be derived from flowing blood cells. Because the venous plexuses in the deep and mid sclera and episclera are thought to be filled partly with clear aqueous humor and partly with blood,[41] it is natural that these venous plexuses can be visualized using OCTA. In contrast, because Schlemm's canal and collector channels do not contain red blood cells under normal conditions, it is expected that they are undetectable by OCTA.

Our data showed that the flow images acquired using AS-OCTA likely reflect components of the AHO pathways. However, several previous studies have suggested that the AHO pathway is more prominent in the nasal quadrant, especially in the inferior nasal segment, than in the temporal quadrant.[32, 33, 42] Although the OCTA-determined vessel density in the nasal quadrant was the highest among the four quadrants analyzed in our study, vessel density in the temporal quadrant was also high; however, the reason for this has not yet been clarified. OCTA theoretically visualizes arteries and veins unrelated to AHO in addition to the venous plexuses involved in AHO. Therefore, OCTA images might include flow signals unrelated to AHO even in the deep layer. This makes sense because as both deep layer OCTA and aqueous angiography show less signals in the periphery than around the limbus (Figure 3), this contrast is more visible with aqueous angiography. However, it should be noted that most of the previous human studies on the post-trabecular AHO pathway were performed in enucleated eyes or invasively.[32, 39, 42] Because OCTA can be performed under non-invasive conditions, future investigations using OCTA might reveal more precise relationships between the intrascleral vasculature and the posttrabecular AHO pathway.

The current study has several limitations. First, this study included only young, healthy participants, and the sample size was small. To reveal the clinical usefulness of AS-OCTA, further large-scale studies are needed. Second, the segmentation algorithm used in this study was commercially available, and dedicated to the posterior segment and not the AS. Delineation of the conjunctival epithelium was performed using the algorithm for the inner limiting membrane. However, the border between the conjunctival and scleral tissues could not be delineated. The superficial layer in the current study was mainly composed of conjunctival tissue, but should contain episcleral and some scleral tissues. In fact, although most deep-layer vessels seemed not to show direct connection with the superficial-layer vessels, some deep-layer vessels seemed to be connected with the superficial-layer vessels (Figure 3, Top row far right and Second row far right). Future improvement of the algorithm specialized for the AS might make OCTA more useful. Third, although AS-OCTA images were successfully acquired, they still had significant noise. Multiple image averaging is known to be helpful in improving image quality in posterior-segment OCTA[27] and AS-OCT, [43, 44] as well as posterior-segment OCT[45]. AS-OCTA imaging with multiple image averaging might be a possible method to improve the image quality in future studies.

In conclusion, OCTA can well visualize and quantitatively measure the functional conjunctival and intrascleral vessels. OCTA images with whole signals were similar to scleral angiography images. Moreover, deep-layer OCTA images had a similar appearance to aqueous angiography images. Deep-layer OCTA flow images have the potential to be useful for posttrabecular AHO evaluation. The application of AS-OCTA to other diseases, including glaucoma, should be investigated in future studies.

Supplementary Material

Refer to Web version on PubMed Central for supplementary material.

Acknowledgements

a. Financial Support:

This work was supported by the Japan Society for the Promotion of Science (JSPS) KAKENHI Grant Number 16K11267 (T.A.), National Institutes of Health, Bethesda, MD Grant Number K08EY024674 (A.S.H.), Research to Prevent Blindness Career Development Award 2016 (A.S.H.), National Eye Institute R01EY029058 (R.N.W.), Core Grant P30EY022589 and an unrestricted grant from Research to Prevent Blindness (New York, N.Y.).

b. Financial Disclosures:

Tadamichi Akagi: Financial support – Alcon, Kowa, Pfizer, Santen, Senju, Canon; Akihito Uji: Financial support – Alcon, Senju, Canon; Alex S. Huang: Research support – Glaukos Corporation, Heidelberg Engineering; Consultant – Allergan; Robert N. Weinreb: Research support – Genentech, Heidelberg Engineering, National Eye Institute, Optos, Optovue; Consultant – Aerie Pharmaceuticals, Alcon, Allergan, Bausch & Lomb, Eyenovia, Novartis, Unity, Valeant; Tatsuya Yamada: None; Manabu Miyata: Financial support – Alcon, Santen; Takanori Kameda: Financial support – Alcon, Senju,Pfizer, Tomey, Santen, Kowa; Hanako Ohashi Ikeda: Financial support – Alcon, Santen, Senju, Wakamoto; Akitaka Tsujikawa: Research support – Pfizer, Bayer, Novartis, Santen, Senju, Alcon, AMO Japan, Hoya, Kowa; Financial support – Pfizer, Bayer, Novartis, Santen, Senju, Alcon, Nidek, AMO Japan, Kowa, Chugai, Sanwa Kagaku.

c. Other Acknowledgements: None.

References

1. Bron AJ, Tripathi RC, Tripathi BJ, eds. Wolff’s anatomy of the eye and orbit, 8th ed. London, UK: Chapman and Hall Medical; 1997:279–307.
2. Owen CG, Newsom RS, Rudnicka AR, et al. Diabetes and the tortuosity of vessels of the bulbar conjunctiva. Ophthalmology 2008;115(6):e27–32. [PubMed: 18423868]
3. Harper RN, Moore MA, Marr MC, et al. Arteriolar rarefaction in the conjunctiva of human essential hypertensives. Microvas Res 1978;16(3):369–372.
4. Abelson MB, Schaefer K. Conjunctivitis of allergic origin: immunologic mechanisms and current approaches to therapy. Surv Ophthalmol 1993;38 Suppl:115–132.
5. Chen W, Batawi HI, Alava JR, et al. Bulbar conjunctival microvascular responses in dry eye. Ocul Surf 2017;15(2):193–201. [PubMed: 28042094]
6. Carreon T, van der Merwe E, Fellman RL, et al. Aqueous outflow - A continuum from trabecular meshwork to episcleral veins. Prog Retin Eye Res 2017;57:108–133. [PubMed: 28028002]
7. Mitsui Y, Matsubara M, Kanagawa M. Fluorescence irido-corneal photography. The Br J Ophthalmol 1969;53(8):505–512. [PubMed: 5811220]
8. Bron AJ, Easty DL. Fluorescein angiography of the globe and anterior segment. Trans Ophthalmol Soc U K 1970;90:339–367. [PubMed: 4933929]
9. Watson PG, Bovey E. Anterior segment fluorescein angiography in the diagnosis of scleral inflammation. Ophthalmology 1985;92(1):1–11.

10. Meyer PA, Watson PG. Low dose fluorescein angiography of the conjunctiva and episclera. Br J Ophthalmol 1987;71(1):2–10. [PubMed: 3814565]
11. Shahidi M, Wanek J, Gaynes B, Wu T. Quantitative assessment of conjunctival microvascular circulation of the human eye. Microvas Res 2010;79(2):109–113.
12. Jiang H, Ye Y, DeBuc DC, et al. Human conjunctival microvasculature assessed with a retinal function imager (RFI). Microvas Res 2013;85:134–137.
13. van Zijderveld R, Ince C, Schlingemann RO. Orthogonal polarization spectral imaging of conjunctival microcirculation. Graefes Arch Clin Exp Ophthalmol 2014;252(5):773–779. [PubMed: 24627137]
14. Marvasti AH, Berry J, Sibug ME, et al. Anterior Segment Scleral Fluorescein Angiography in the Evaluation of Ciliary Body Neoplasm: Two Case Reports. Case Rep Ophthalmol 2016;7(1):30–38. [PubMed: 26889157]
15. Mariampillai A, Standish BA, Moriyama EH, et al. Speckle variance detection of microvasculature using swept-source optical coherence tomography. Opt Lett 2008;33(13):1530–1532. [PubMed: 18594688]
16. Jia Y, Tan O, Tokayer J, et al. Split-spectrum amplitude-decorrelation angiography with optical coherence tomography. Opt Express 2012;20(4):4710–4725. [PubMed: 22418228]
17. Jia Y, Wei E, Wang X, et al. Optical coherence tomography angiography of optic disc perfusion in glaucoma. Ophthalmology 2014;121(7):1322–1332. [PubMed: 24629312]
18. Liu L, Jia Y, Takusagawa HL, et al. Optical Coherence Tomography Angiography of the Peripapillary Retina in Glaucoma. JAMA Ophthalmol 2015;133(9):1045–1052. [PubMed: 26203793]
19. Akagi T, Iida Y, Nakanishi H, et al. Microvascular Density in Glaucomatous Eyes with Hemifield Visual Field Defects: An Optical Coherence Tomography Angiography Study. Am J Ophthalmol 2016;168:237–249. [PubMed: 27296492]
20. Yarmohammadi A, Zangwill LM, Diniz-Filho A, et al. Relationship between Optical Coherence Tomography Angiography Vessel Density and Severity of Visual Field Loss in Glaucoma. Ophthalmology 2016;123(12):2498–2508. [PubMed: 27726964]
21. Uji A, Balasubramanian S, Lei J, et al. Choriocapillaris Imaging Using Multiple En Face Optical Coherence Tomography Angiography Image Averaging. JAMA Ophthalmol 2017;135(11):1197–1204. [PubMed: 28983552]
22. Ang M, Sim DA, Keane PA, et al. Optical Coherence Tomography Angiography for Anterior Segment Vasculature Imaging. Ophthalmology 2015;122(9):1740–1747. [PubMed: 26088621]
23. Ang M, Cai Y, Shahipasand S, et al. En face optical coherence tomography angiography for corneal neovascularisation. Br J Ophthalmol 2016;100(5):616–621. [PubMed: 26311064]
24. Chien JL, Sioufi K, Ferenczy S, et al. Optical Coherence Tomography AngiographyFeatures of Iris Racemose Hemangioma in 4 Cases. JAMA Ophthalmol 2017;135(10):1106–1110. [PubMed: 28910426]
25. Skalet AH, Li Y, Lu CD, et al. Optical Coherence Tomography Angiography Characteristics of Iris Melanocytic Tumors. Ophthalmology 2017;124(2):197–204. [PubMed: 27856029]
26. Kim AY, Chu Z, Shahidzadeh A, et al. Quantifying Microvascular Density and Morphology in Diabetic Retinopathy Using Spectral-Domain Optical Coherence Tomography Angiography. Invest Ophthalmol Vis Sci 2016;57(9):OCT362–370. [PubMed: 27409494]
27. Uji A, Balasubramanian S, Lei J, et al. Impact of Multiple En Face Image Averaging on Quantitative Assessment from Optical Coherence Tomography Angiography Images. Ophthalmology 2017;124(7):944–952. [PubMed: 28318637]
28. Uji A, Murakami T, Suzuma K, et al. Influence of Vitrectomy Surgery on the Integrity of Outer Retinal Layers in Diabetic Macular Edema. Retina 2018;38(1):163–172. [PubMed: 28263219]
29. Reif R, Qin J, An L, et al. Quantifying optical microangiography images obtained from a spectral domain optical coherence tomography system. Int J Biomed Imaging 2012;2012:509783. [PubMed: 22792084]
30. Zahid S, Dolz-Marco R, Freund KB, et al. Fractal Dimensional Analysis of Optical Coherence Tomography Angiography in Eyes With Diabetic Retinopathy. Invest Ophthalmol Vis Sci 2016;57(11):4940–4947. [PubMed: 27654421]

31. Huang AS, Camp A, Xu BY, et al. Aqueous Angiography: Aqueous Humor Outflow Imaging in Live Human Subjects. Ophthalmology 2017;124(6):1249–1251. [PubMed: 28461013]
32. Huang AS, Li M, Yang D, et al. Aqueous Angiography in Living Nonhuman Primates Shows Segmental, Pulsatile, and Dynamic Angiographic Aqueous Humor Outflow. Ophthalmology 2017;124(8):793–803. [PubMed: 28237425]
33. Johnstone M, Martin E, Jamil A. Pulsatile flow into the aqueous veins: manifestations in normal and glaucomatous eyes. Exp Eye Res 2011;92(5):318–327. [PubMed: 21440541]
34. Kagemann L, Wollstein G, Ishikawa H, et al. Identification and assessment of Schlemm's canal by spectral-domain optical coherence tomography. Invest Ophthalmol Vis Sci 2010;51(8):4054–4059. [PubMed: 20237244]
35. Francis AW, Kagemann L, Wollstein G, et al. Morphometric analysis of aqueous humor outflow structures with spectral-domain optical coherence tomography. Invest Ophthalmol Vis Sci 2012;53(9):5198–5207. [PubMed: 22499987]
36. Uji A, Muraoka Y, Yoshimura N. In Vivo Identification of the Posttrabecular Aqueous Outflow Pathway Using Swept-Source Optical Coherence Tomography. Invest Ophthalmol Vis Sci 2016;57(10):4162–4169. [PubMed: 27537266]
37. Yoshikawa M, Akagi T, Uji A, et al. Pilot study assessing the structural changes in posttrabecular aqueous humor outflow pathway after trabecular meshwork surgery using swept-source optical coherence tomography. PLoS One 2018;13(6):e0199739. [PubMed: 29953502]
38. Hann CR, Bentley MD, Vercnocke A, et al. Imaging the aqueous humor outflow pathway in human eyes by three-dimensional micro-computed tomography (3D micro-CT). Exp Eye Res 2011;92(2): 104–111. [PubMed: 21187085]
39. Fellman RL, Feuer WJ, Grover DS. Episcleral Venous Fluid Wave Correlates with Trabectome Outcomes: Intraoperative Evaluation of the Trabecular Outflow Pathway. Ophthalmology 2015;122(12):2385–2391 e1. [PubMed: 26477844]
40. Huang AS, Francis BA, Weinreb RN. Structural and functional imaging of aqueous humour outflow: a review. Clin Exp Ophthalmol 2017.
41. Ascher K Aqueous veins: preliminary note. Am J Ophthalmol 1942;25:31–38.
42. Cha ED, Xu J, Gong L, Gong H. Variations in active outflow along the trabecular outflow pathway. Exp Eye Res 2016;146:354–360. [PubMed: 26775054]
43. Akagi T, Uji A, Yoshimura N. Glaucoma Tube Changes After Suture Lysis Assessed by High-Resolution Anterior Segment Optical Coherence Tomography. JAMA Ophthalmol 2016;134(2):e153674. [PubMed: 26869130]
44. Akagi T, Nakano E, Nakanishi H, et al. Transient Ciliochoroidal Detachment After Ab Interno Trabeculotomy for Open-Angle Glaucoma: A Prospective Anterior-Segment Optical Coherence Tomography Study. JAMA Ophthalmol 2016;134(3):304–311. [PubMed: 26823200]
45. Sakamoto A, Hangai M, Yoshimura N. Spectral-domain optical coherence tomography with multiple B-scan averaging for enhanced imaging of retinal diseases. Ophthalmology 2008;115(6): 1071–1078 e7. [PubMed: 18061270]

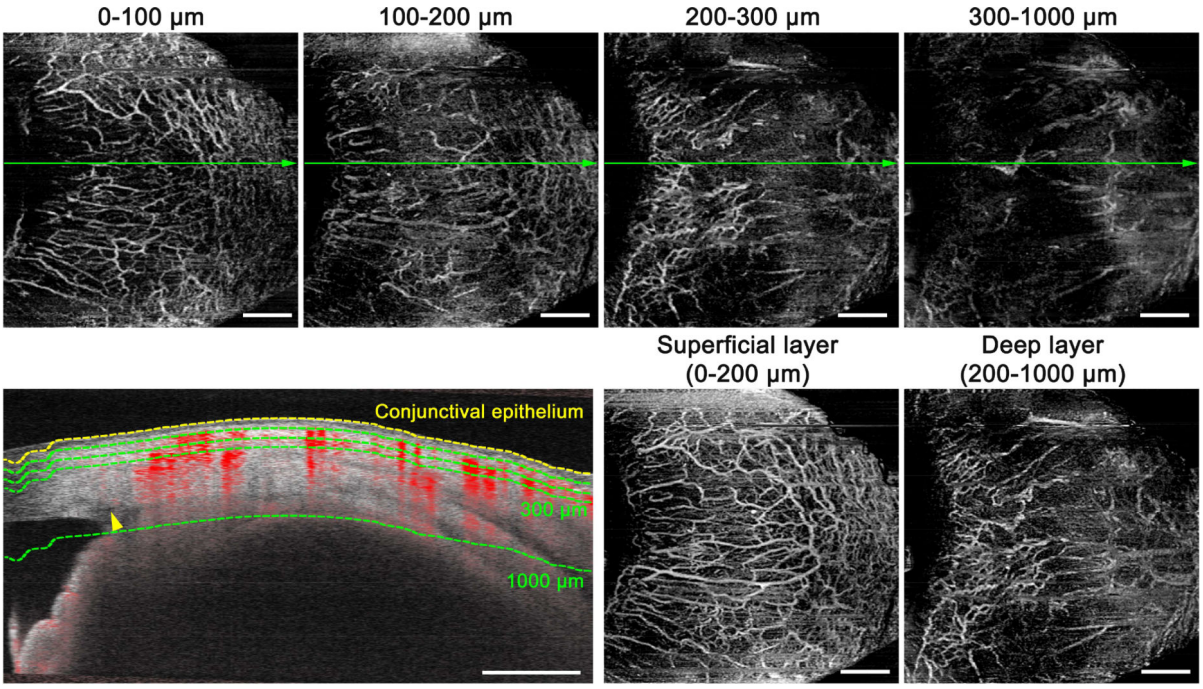

FIGURE 1.

Delineation of the superficial and deep layers on anterior-segment optical coherence tomography angiography (OCTA) images of the corneal limbus in the nasal quadrant. (Top row) En face maximum projection images from the conjunctival epithelium to a depth of 100 μm, from a depth of 100 μm to 200 μm, from a depth of 200 μm to 300 μm, and from a depth of 300 μm to 1000 μm from the conjunctival epithelium. (Bottom left) Cross-sectional angiography images overlying the B-scan image acquired at the green line in Top row. Yellow dotted line is determined as the conjunctival epithelium, and green dotted lines are as a depth of 100, 200, 300, and 1000 μm from the conjunctival epithelium. A yellow arrowhead shows Schlemm's canal, which does not show any OCTA signals. (Bottom near right and Bottom far right) Superficial- (from the conjunctival epithelium to a depth of 200 μm) and deep-layer (from a depth of 200 μm to 1000 μm from the conjunctival epithelium) flow images are mainly composed of the conjunctival and intrascleral vessels, respectively. Scale bar = 1 mm.

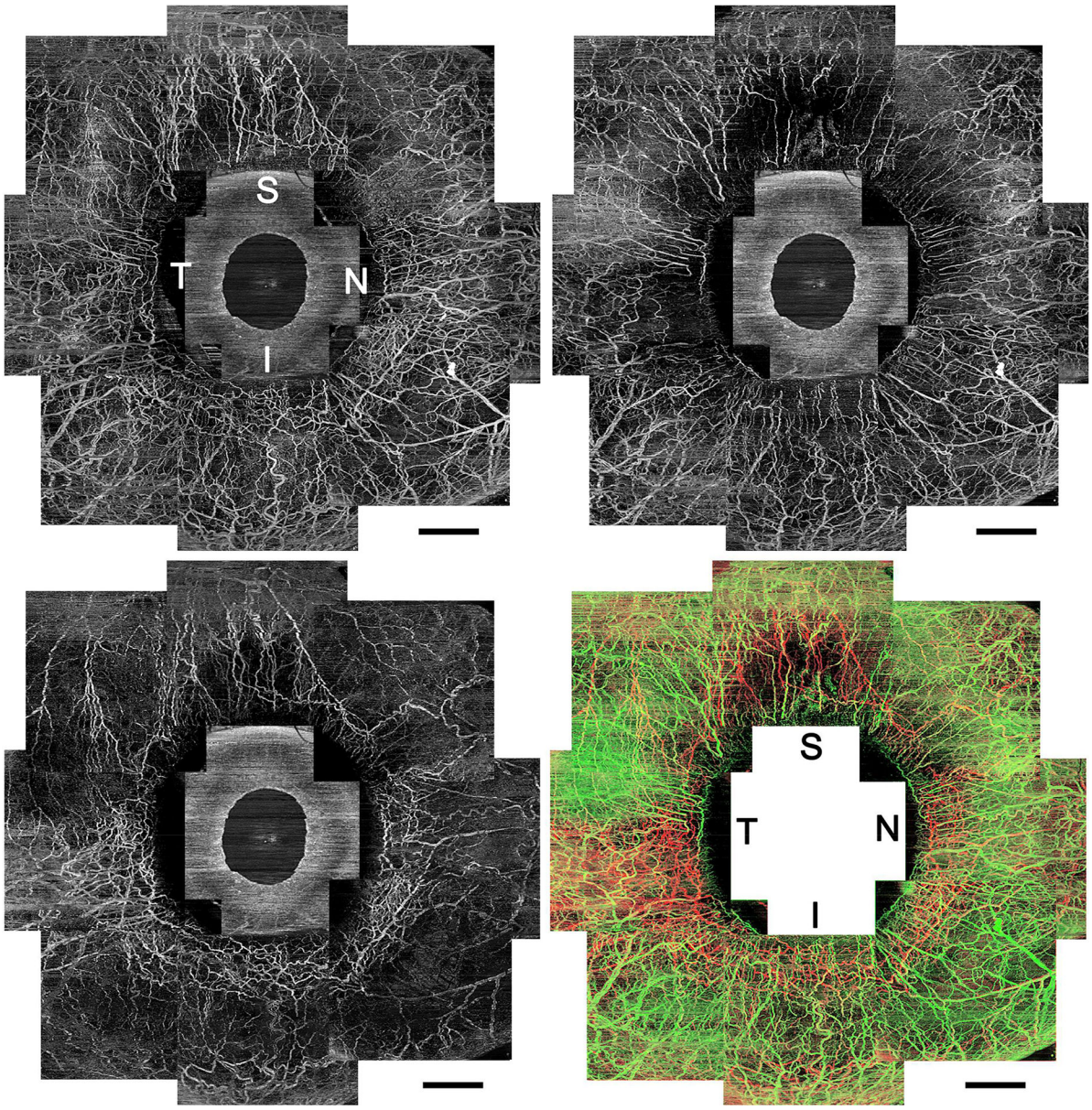

FIGURE 2.

Circumferential vasculature panoramic images acquired using optical coherence tomography angiography (OCTA) of the right eye in a healthy participant. (Top left) An OCTA en face image with whole OCTA signals. (Top right) A superficial-layer flow image with en face maximum projection from the conjunctival epithelium to a depth of 200 μm. Vessels distribute homogeneously from the limbus to the periphery. (Bottom left) A deep-layer flow image with en face maximum projection from a depth of 200 μm to 1000 μm from the conjunctival epithelium. Deep or mid scleral venous plexuses are densely arranged around the limbus, and fewer vessels extend to the periphery, which shows Y-shaped sectoral patterns. (Bottom right) Merged vasculature image shown in different colors (superficial layer network, green; deep layer, red; merged, yellow). It should be noted that the green and

red vessels are separately visualized. I = inferior; N = nasal; S = superior; T = temporal. Scale bar = 2 mm.

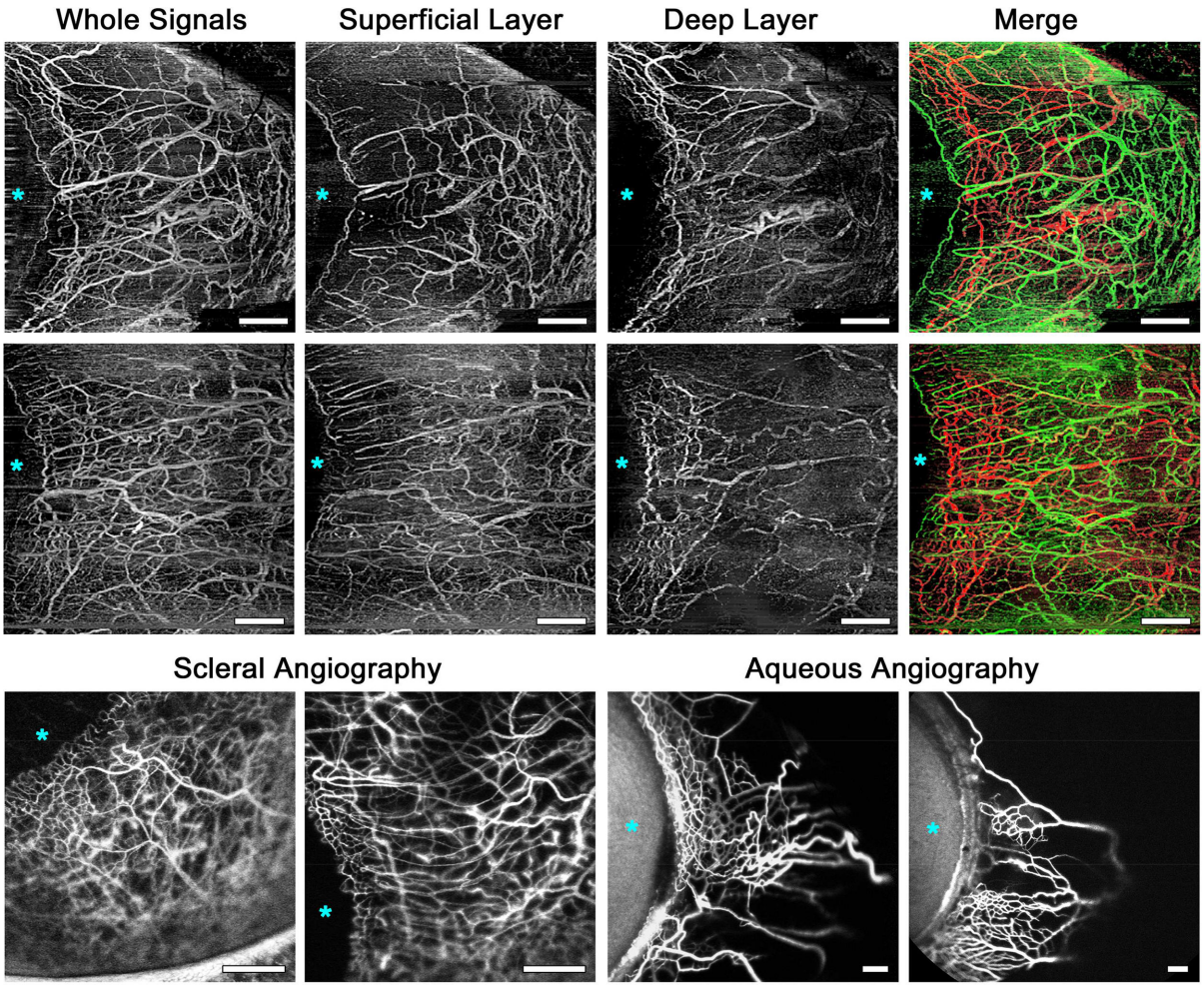

FIGURE 3.

Comparison among optical coherence tomography angiography (OCTA) images, fluorescein scleral angiography images, and indocyanine green (ICG) aqueous angiography images. (Top row and Second row) OCTA flow images in the nasal quadrants of the right eyes in two healthy subjects. (Top row far left and Second row far left) OCTA flow images with whole signals. (Top row near left and Second row near left) Superficial-layer OCTA flow images show dense vasculature at the periphery as well as around the limbus. (Top row near right and Second row near right) Deep-layer OCTA flow images show sectoral patterns, which are composed of dense venous plexuses around the limbus and fewer vessels extending to the periphery. (Top row far right and Second row far right) Merged OCTA vasculature images shown in different colors (superficial layer network, green; deep layer, red) for better visualization of the connection between the layers. (Bottom row far left and Bottom row near left) Scleral angiography images using fluorescein in the temporal (Bottom row far left) and nasal quadrant (Bottom row near left, mirror-reversed image) of two left eyes without any ocular disease, which were taken about 35–40 seconds after the fluorescein intravenous injection. These images are similar to the OCTA images with whole signals showing vascularity around the limbus and in the periphery. (Bottom row near right and Bottom row far right) Aqueous angiography images using ICG of the nasal quadrants of two left eyes

(mirror-reversed images), which were taken about 1.5 minutes (Bottom row near right) and 3.0 minutes (Bottom row far right) after intra-aqueous ICG injection. The angiographically positive patterns are similar to those of deep-layer OCTA flow images with more vascularity around the limbus compared to the periphery. Asterisks indicate location of the cornea. The OCTA, scleral angiography, and aqueous angiography images were obtained from the different subjects. Scale bar = 1 mm.

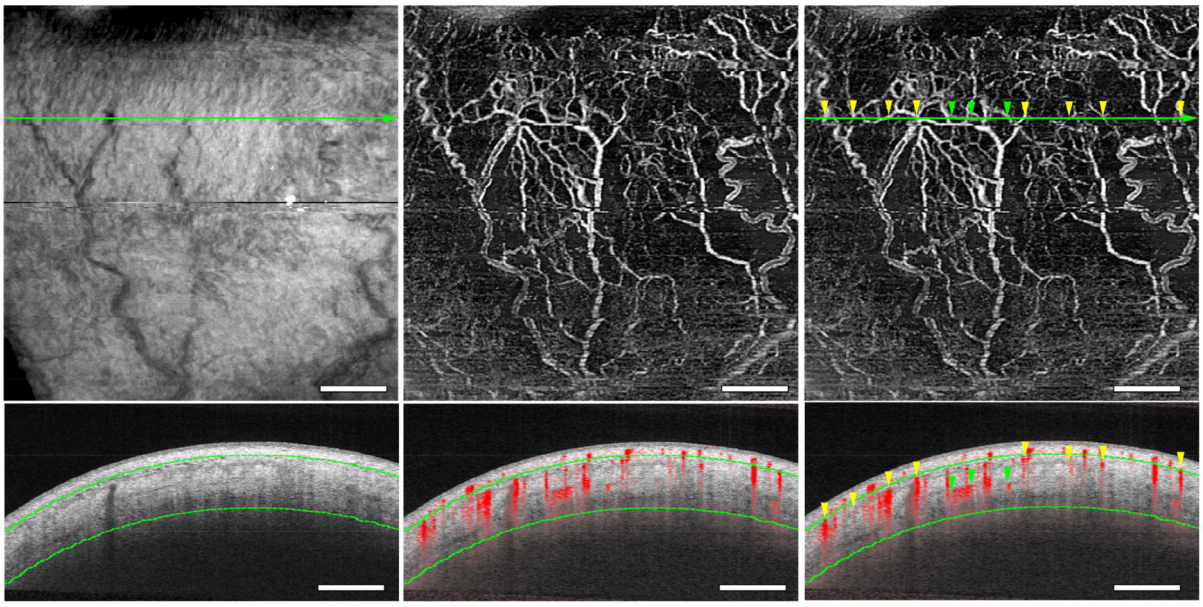

FIGURE 4.

Optical coherence tomography (OCT) luminal structures and OCT angiography (OCTA) flow signals. Deep-layer OCT (Top left) and OCTA (Top middle and Top right) en face flow images in the inferior quadrant. (Bottom row) A B-scan image (Bottom left) and a cross-sectional angiography image overlying the B-scan image (Bottom middle and Top right) acquired at the green line in Top row. Luminal structures are identical in OCT images, and OCTA signals correspond to the episcleral and intrascleral luminal structures (yellow and green arrowheads, respectively). Green dotted lines are determined as a depth of 200 μm and 1000 μm from the conjunctival epithelium. Scale bar = 1 mm.

Table 1.

Comparisons of Vasculature Parameters among Different Locations using Optical Coherence Tomography Angiography Imaging

	Average	Nasal (N)	Temporal (T)	Inferior (I)	Superior (S)	ANOVA	Post Hoc†
Superficial Layer						*P* Value	
Vessel density (%)	27.4±3.0	30.6±3.1	26.7±4.4	25.6±4.6	26.8±4.4	0.054	
Vessel length density (%)	4.67±0.48	5.00±0.40	4.60±0.83	4.26±0.69	4.83±0.87	0.069	
Vessel diameter index	17.2±0.6	18.0±0.8	17.0±0.4	17.6±1.2	16.3±1.1	0.003	**N>S**
Fractal dimension	1.333±0.034	1.353±0.028	1.329±0.060	1.309±0.058	1.341±0.060	0.32	
Deep Layer Vessel density (%)	23.0±2.1	25.8±3.2	24.6±3.0	20.9±3.5	20.6±4.1	0.003	**N>S**
Vessel length density (%)	3.88±0.35	4.49±0.56	4.42±0.62	3.41±0.68	3.19±0.66	<0.001	**N>I,S T>I,S**
Vessel diameter index	17.6±0.7	16.8±0.8	16.3±0.7	18.1±1.2	19.0±1.5	<0.001	**N<S T<S,I**
Fractal dimension	1.280±0.028	1.335±0.036	1.328±0.045	1.240±0.067	1.217±0.059	<0.001	**N>S,I T>S,I**

Data are mean ± standard deviation.

†Significant differences in Tukey's honestly significant differences after Bonferroni corrections are shown.